Computer Assisted Mechanics and Engineering Sciences, 9: 205–221, 2002.


# Global optimization in material functions identification for voided media plastic flow

Zdzisław Nowak
*Institute of Fundamental Technological Research, Polish Academy of Sciences*
*ul. Świętokrzyska 21, 00-049 Warsaw, Poland*

Andrzej Stachurski
*Institute of Control and Computation Engineering, Warsaw University of Technology*
*ul. Nowowiejska 15/19, 00-665 Warsaw, Poland*

(Received June 5, 2000)

The aim of this paper is to present an application of the global optimization method of Boender et al. to a material function identification in a mechanical problem. These material functions are found in the evolution equation for a volume void fraction parameter describing nucleation and growth of microvoids in the flow of porous ductile solids and they play an important role in proper constitutive modelling of postcritical behaviour and fracture. In the evolution equation a plastic strain controlled nucleation process is simulated and uniaxial tension deformation history is considered. In nonlinear regression the minimization of the mean squares functional is assumed. The problem is treated directly as a global optimization one. The necessity of the use of a global optimization approach follows from the hypothesis that there can exist many local minima in the considered problem. The possibility of the existence of many local minima is not usually taken into account. The global optimization method of Boender et al. was applied to minimize the least squares functional. We determine the material functions parameters on the basis of the given Fischer's [8] experimental data set. This data set has been obtained for axisymmetric tension of steel specimens. The results of numerical calculations presented in the paper proved the validity of the hypothesis about the existence of many local minima.

**Keywords:** plastic flow of voided media, material functions identification, global optimization, nonlinear regression, nonlinear programming

## 1. Introduction

The Levenberg–Marquardt method (cf. Levenberg [13], Marquardt [14]) is usually used to minimize the least squares function with respect to the unknown parameters to be estimated. The possibility of the existence of many local minima is usually not noted. The Levenberg–Marquardt algorithm converges to one of the existing minima. The limit point depends on the starting point. However, many local minima may be expected in our case, since the parameters appear nonlinearly in the considered model.

In many mechanical problems of plastic flow and fracture of dissipative solids the intrinsic microdamage effects are observed. In literature, to describe the intrinsic microdamage effects a set of the internal state variables or one porosity parameter $\xi$ and some material constants are introduced. In such constitutive models all parameters have to be determined by the proposed evolution equation. The evolution equation for porosity parameter $\xi$ has to describe the nucleation and growth mechanisms of microvoids.

The formation of microvoids in commercial grade materials is attributed to the presence of inhomogeneities in the form of dispersed inclusions or second phases. This fact has been indicated by Argon, Im and Safoglu [3] and Argon and Im [2]. The microvoids appear either as cracks in the

particles or as failure of the particle-matrix interfacial bonding. The actual microvoid morphology depends upon the interrelation of various microstructural parameters as well as the local deformation state. In very high purity materials the voids were observed to nucleate at dislocation structures which had evolved into cell boundaries. Void formation may be associated with diffusion control processes in which grain boundaries act as sinks or sources for vacancies.

The volume fraction of microvoids $\xi$ as a function of equivalent plastic strain $\bar{\epsilon}_p$ for carbon steel given by Fisher [8] is presented in Section 5. Since this measure of voids is to be used in our forthcoming analysis, it is worth separating the nucleation and growth parts from the full measure of $\xi$. As in Perzyna and Nowak [17] the relationship between $\xi^n$, $\xi^g$ and $\bar{\epsilon}_p$ can be obtained, and it is realised in Section 5.

It is postulated that the evolution equation for porosity parameter has the form (cf. [16, 17])

$$(\dot{\xi}) = (\dot{\xi})_{\text{nucleation}} + (\dot{\xi})_{\text{growth}} = \boldsymbol{h}(\bar{\epsilon}_p\,,\,\xi)\,\boldsymbol{\sigma} : \mathbf{D}^p + \boldsymbol{l}(\bar{\epsilon}_p\,,\,\xi)\,\dot{J}_1 + \boldsymbol{g}(\bar{\epsilon}_p\,,\,\xi)\,\mathbf{D}^p : \mathbf{I} \tag{1}$$

where $\boldsymbol{h}$, $\boldsymbol{l}$, $\boldsymbol{g}$ are the material functions, $\mathbf{I}$ denotes the unit tensor, $\bar{\epsilon}_p$ is the equivalent plastic strain, $\boldsymbol{\sigma}$ is the Cauchy stress tensor, $\mathbf{D}^p$ denotes the plastic rate of the deformation tensor and $J_1 = \text{tr}(\boldsymbol{\sigma})$.

It is assumed that the nucleation mechanism occurs mainly at second-phase particles, by decohesion of the particle–matrix interface and by the particle cracking. The growth process is postulated to be controlled only by the plastic flow phenomenon. Both assumptions are justified by the experimental observation results for metals (cf. a review paper by Needleman and Rice [15]).

The first term in the evolution equation (1) for the porosity parameter $\xi$ describes debonding of second-phase particles from the matrix as the plastic work progressively increases and the second term is responsible for the cracking of the second-phase particles. The nucleation material functions $\boldsymbol{h}$ and $\boldsymbol{l}$ depend on the equivalent plastic deformation $\bar{\epsilon}_p$ and the porosity $\xi$. The third term in Eq. (1) is related to the growth mechanism. It is assumed that the growth material function $\boldsymbol{g}$ depends on the equivalent plastic deformation $\bar{\epsilon}_p$ and porosity $\xi$. Furthermore it is assumed that material function $\boldsymbol{l} = 0$.

The form of the evolution equation (1) obviously requires further study and improvements. In this paper we focus on the identification of material functions with the Fisher's [8] experimental data. Some parts of our work parallel and extend what has been carried out by Perzyna and Nowak [17], where both material functions $\boldsymbol{h}$ and $\boldsymbol{g}$ are also determined.

In this paper we focus on the traditional least squares formulation of the identification problem where the sum of the second power of deviations of the calculated and measured values is minimized. We have expected the existence of many local minima in our problem. Therefore we have prepared in standard ANSI C language the global minimization procedure of Boender et al. in the form presented in Törn and Žilinskas [23]. It combines the clusterization approach with the local minimization. Locally we have used the BFGS quasi-Newton method with the numerical gradient estimation. The BFGS method is an unconstrained optimization method; however, in our implementation we have introduced box constraints on the parameters.

The Gurson's voided media plastic flow model itself is a set of differential equations. Involvement of the Bridgman's solution for the stress state reduces this set to one differential equation. To obtain the calculated porosity parameter $\xi$ we had to solve poorly conditioned differential evolution equation (1). Finally we have decided to solve it by means of the Rosenbrock method for stiff differential equations. Numerical algorithms mentioned above are briefly presented in Section 6.

The material functions formulae are described and the resulting least squares problem is introduced in Section 4. Data used for parameter estimation are presented in Section 5. The computational results are shown and discussed in Section 7. Some conclusions and observations are also stated. The presentation of the whole set of local minima in the included tables of results is restricted to ten sectors due to the lack of space. Finally, Section 8 contains some concluding remarks.

## 2. Formulation of the identification problem

Our task is to find the optimal estimates of the unknown parameters in the material functions $\boldsymbol{h}$ and $\boldsymbol{g}$ which appear in equation (1). It is assumed that the nucleation mechanism is controlled by the plastic strain only and material function $l = 0$ in Eq. (1). We start with the presentation of the general approach to parameter identification. When using the standard least squares approach usually the second power of the distance between the observed output values $Y_i$ and the calculated output values $\tilde{Y}_i$ ($\tilde{Y}_i = F(\bar{\epsilon}_{pi}, x)$) is minimized. Here $F$ represents the assumed model and it connects the input variables values with the output values, the independent variables, $\bar{\epsilon}_{pi}$, and accordingly $x$ – the unknown parameters

$$\min_{x \in V} \|Y - \tilde{Y}\|^2 \tag{2}$$

where $V \subset R^n$ denotes the set of admissible parameters values ($n$ is the number of the unknown parameters to be identified). Substitution of the formula $\tilde{Y}_i = F(\bar{\epsilon}_{pi}, x)$ into (2) yields

$$\min_{x \in V} \sum_{i=1}^{M} \{Y_i - F(\bar{\epsilon}_{pi}, x)\}^2. \tag{3}$$

The second term in Eq. (3) represents the calculated output values $\tilde{Y}_i$, and $M$ is the number of observations (measured input and corresponding output values). In (3), the second power of the distance is used. If $V = R^n$ (the unconstrained case), the minimization of the distance is equivalent to the minimization of its second power. Therefore, in the least squares method usually the second power of the distance in the observations space is minimized.

In our case the calculated output is obtained as a result of the integration of an ordinary differential equation, where on the left-hand appears its derivative with respect to the input $\bar{\epsilon}_p$. The right-hand side of the differential equation depends on the input and output variables and on the unknown parameters. Unknown parameters appear exclusively in the so-called material functions being a part of the right-hand side of the differential equation. See for details Sections 3 and 4.

The parameters should belong to the set V of feasible values of parameters, defined in Section 4.

## 3. Porosity model

### 3.1. Porosity evolution at the neck

In the following considerations the uniaxial test is assumed for room temperature. We assume, following Hill [12], that after a neck has been formed in a cylindrical tensile specimen the distribution of the stress across a transverse section is not uniform. Our analysis is based on the constitutive relation for the porous plastic solids. We put it into the form introduced by Rudnicki and Rice [19].

We have assumed an augmented version of the Gurson's porous material model [10] with a following porosity evolution (1)

$$\dot{\xi} = \boldsymbol{h} \frac{1}{1-\xi} \operatorname{tr}(\boldsymbol{\sigma} \mathbf{D}^p) + \boldsymbol{g}(1-\xi) \operatorname{tr}(\mathbf{D}^p). \tag{4}$$

It is the Gurson's form of the equation of porosity evolution with varying $\boldsymbol{g}$ as proposed by Perzyna [16]. Varying $\boldsymbol{g}$ was meant to reflect the influence of voids from the neighbourhood on the growth of a particular void. In Eq. (4) plastic strain controlled nucleation criterion suggested by the Gurson's [10] analysis of experimental data obtained by Gurland [11] is assumed. The nucleation of microvoids is not dependent on the hydrostatic stress. We assume that $\boldsymbol{h}$ and $\boldsymbol{g}$ are functions depending on plastic strain and unknown parameters.

Our purpose is to determine the material functions $\boldsymbol{h}$ and $\boldsymbol{g}$ on the basis of the given experimental data set. We have tested many formulae on $\boldsymbol{h}$ and $\boldsymbol{g}$ described in Section 4.

Let us consider an element of the solid to be subjected to all around displacement boundary conditions. Attention here is focused on an element at the center of the neck which is formed in an axisymmetric tensile specimen. The element is assumed to be sufficiently small to be regarded as homogeneously deformed, yet large enough compared with relevant microstructural length scales (e.g. grain size, inclusion and void spacing) to be treated within the continuum framework employed here. At the neck there exists a complex state of stress and maximal deformations. A material point is identified by the Cartesian convected coordinates $x^i$ $(i = 1, 2, 3)$ in the reference state. In the current deformed state the coordinates of the material point, relative to the cartesian frame, are denoted by $\bar{x}^i$. To implement the numerical method we applied the incremental analysis procedure (cf. Perzyna and Nowak [17]) in which the evolution equation (4) for a porous plastic solid has the following form

$$\frac{\dot{\xi}}{\dot{\bar{\varepsilon}}_p} = \left[ h \frac{1}{1-\xi} \left( \lambda_1 \frac{\sigma_{xx}}{\sigma_{zz}} + \lambda_2 \frac{\sigma_{yy}}{\sigma_{zz}} + 1 \right) + g(1-\xi)(\lambda_1 + \lambda_2 + 1) \right] \frac{1}{\sqrt{\lambda^*}} \tag{5}$$

where

$$\lambda_1 = \frac{\dot{E}^p_{xx}}{\dot{E}^p_{zz}}, \qquad \lambda_2 = \frac{\dot{E}^p_{yy}}{\dot{E}^p_{zz}}, \qquad \text{and} \qquad \lambda^* = \frac{2}{3}[(\lambda_1)^2 + (\lambda_2)^2 + 1].$$

### 3.2. Stress state at the neck

We employ Bridgman's [5] solution for the stress state at the center of the minimum section of the tensile cylindrical sample. This analysis of stress distribution is obtained with a radical simplification based on the experimental observation that the elements in the minimum section are deformed uniformly (at any rate). As consequence of such assumption, the circumferential strain rate $\dot{E}_{yy}$ is equal to radial strain rate $\dot{E}_{xx}$ in the minimum section and it follows that $\sigma_{xx} = \sigma_{yy}$ there (cp. Hill [12, p. 273]). After inserting this in the equilibrium equations and combining with the yield condition (provided the influence of a hydrostatic stress and the influence of porosity on yielding is neglected; the yield condition in Bridgman's analysis is simply $\sigma_{zz} - \sigma_{xx} = \bar{\sigma}$, when $z = 0$),

$$\sigma_{xx} = \sigma_{yy} = \bar{\sigma} \ln\left( \frac{R^2 + 2R\rho_R}{2R\rho_R} \right), \qquad \sigma_{zz} = \bar{\sigma} \left( 1 + \ln\left( \frac{R^2 + 2R\rho_R}{2R\rho_R} \right) \right), \qquad \text{for } x,\ y,\ z = 0. \tag{6}$$

The analytical expression for the stress depends on the matrix flow stress, $\bar{\sigma}$ and the geometry of the neck, i.e. on the ratio $\frac{R}{\rho_R}$, where $R$ is the radius of the minimum section and $\rho_R$ is the neck contour radius. Similarly as in Saje, Pan and Needleman [20], it is assumed that

$$\begin{aligned} \frac{R}{\rho_R} &= 0.833(\bar{\varepsilon}_p - 0.2), && \text{for } \bar{\varepsilon}_p \geq 0.2, \\ \frac{R}{\rho_R} &= 0.0, && \text{for } \bar{\varepsilon}_p < 0.2. \end{aligned} \tag{7}$$

Taking Eq. (7) into account in the Bridgman solution we obtain for axisymmetric tension

$$\frac{\sigma_{xx}}{\sigma_{zz}} = \frac{\sigma_{yy}}{\sigma_{zz}} = \lambda \tag{8}$$

where

$$\lambda = \frac{\ln\left( \dfrac{R^2 + 2R\rho_R}{2R\rho_R} \right)}{1 + \ln\left( \dfrac{R^2 + 2R\rho_R}{2R\rho_R} \right)}. \tag{9}$$

Furthermore, we have assumed the constitutive relation for the porous plastic solids introduced by Gurson [10]. This constitutive relation can be put into the form introduced by Rudnicki and Rice [19], $\dot{E}_{ij} = \frac{1}{H} P_{ij} Q_{kl} \overset{\nabla}{\sigma}{}^{kl}$, where $\overset{\nabla}{\sigma}$ is the Jaumann rate-of-change of Cauchy stress. Using this relation we can determine $\lambda_1$ and $\lambda_2$,

$$\lambda_1 = \lambda_2 = \frac{3S_{xx} + \bar{\sigma}\alpha}{3S_{zz} + \bar{\sigma}\alpha}, \tag{10}$$

where $S_{ij} = \sigma_{ij} - \frac{1}{3}\sigma_{kk}\sigma_{ij}$ and

$$\alpha = \xi \sinh\left(\frac{\sigma_{kk}}{2\bar{\sigma}}\right). \tag{11}$$

## 4. Material functions

There exist certain requirements upon the shape of the material function $\boldsymbol{h}$. We started trying to follow the ideas of Chu and Needleman [6]. So, as the Case I, the Gauss normal distribution function for function $\boldsymbol{h}$ was applied,

$$\boldsymbol{h}(\bar{\epsilon}_p, a_1, b_1, c_1) = \frac{a_1}{b_1\sqrt{2\pi}} \exp\left(-\frac{1}{2}\left[\frac{\bar{\epsilon}_p - c_1}{b_1}\right]^2\right), \tag{12}$$

where $a_1$, $b_1$, $c_1$ are the unknown parameters. All of these parameters have their mechanical meaning. Namely, $a_1$ denotes the maximum value of the porosity parameter, $b_1$ is the width of the voids distribution region and $c_1$ represents the value of the equivalent plastic strain $\bar{\epsilon}_p$ at the time moment when the porosity parameter reaches its maximal value.

The second material function $\boldsymbol{g}$ describing the growth of microvoids must be uniformly equal to 1 when initial void or voids are isolated in an unbounded matrix. It means that voids do not interact, no nucleation of new voids and no coalescence of voids in growth process are considered. These three phenomena are closely interrelated and can occur simultaneously. In our analysis function $\boldsymbol{g}$ is not necessarily constant. In Case I the following formula for function $\boldsymbol{g}$ (as in Perzyna and Nowak [17]) was used

$$\boldsymbol{g}(\bar{\epsilon}_p, a_2, b_2, c_2) = a_2 \exp\left[b_2(\bar{\epsilon}_p)^{c_2}\right]. \tag{13}$$

Unfortunately, in this case, the mechanical interpretation of the unknown parameters $a_2$, $b_2$ and $c_2$ is not so clear.

The identification was also carried out with two other different forms of material functions $\boldsymbol{h}$ and $\boldsymbol{g}$.

In Case II:

$$\boldsymbol{h} = a_1(\bar{\epsilon}_p)^{b_1} \exp(c_1\bar{\epsilon}_p), \tag{14}$$

$$\boldsymbol{g} = a_2\sqrt{(\bar{\epsilon}_p)^2 + b_2(\bar{\epsilon}_p) + c_2}, \tag{15}$$

In Case III:

$$\boldsymbol{h} = a_1[1 + \tanh(b_1\bar{\epsilon}_p + c_1)], \tag{16}$$

$$\boldsymbol{g} = \frac{a_2}{b_2 - \bar{\epsilon}_p}. \tag{17}$$

We will refer to the case with $\boldsymbol{h}$ given by Eq. (12) and $\boldsymbol{g}$ given by Eq. (13) as Case I throughout the rest of the paper. Our aim in considering various forms of material functions was to obtain

the "best" fitting of the model to the data in the sense of the lowest value of the mean squares functional (3)). Furthermore, it is necessary to impose some bounds on the parameters to assure their appropriate mechanical interpretation and to avoid overflows in calculations (specially for $g$ function). In our computations we have used the following strategy – at the beginning a broad range of feasible parameters was assumed, e.g.

$$\begin{aligned}
&\text{In case I:} && 0.01 \le a_1 \le 0.05, && 0.2 \le b_1 \le 0.6, && 0.9 \le c_1 \le 1.3,\\
&&& 1.0 \le a_2 \le 1.5, && 0.01 \le b_2 \le 0.3, && 0.01 \le c_2 \le 0.2,\\
&\text{In case II:} && 0.0001 \le a_1 \le 0.1, && 1.0 \le b_1 \le 1.5, && 1.0 \le c_1 \le 1.4,\\
&&& 0.01 \le a_2 \le 0.6, && 0.1 \le b_2 \le 0.5, && 0.8 \le c_2 \le 1.0,\\
&\text{In case III:} && 0.001 \le a_1 \le 0.1, && 2.5 \le b_1 \le 5.0, && -4.0 \le c_1 \le 0.01,\\
&&& 1.0 \le a_2 \le 2.5, && 3.0 \le b_2 \le 4.5.
\end{aligned}$$

Next, we have continued our calculations taking at the next steps small intervals containing the previously found optimal values of parameters as their new feasible ranges. At each such main step we have found several local optima. Many of them had some variables equal to their bounds. Because of that we have adopted special strategy consisting in subsequent minimizations with restricted range of parameters. It gave us an opportunity to better explore the whole range of parameters we were interested in. The second and very important reason for such strategy was the large computational effort and memory required to store many local minima and points leading towards them if we decided to run the program assuming excessively broad range of parameters. The third and not less important reason were numerical difficulties encountered in the integration of the differential equation. Its right-hand side contains singularity and is very sensitive even with respect to relatively small changes in some parameters. Very often the integration procedure stopped calculations with an unpleasant message that stepsize is insignificant. It was simply impossible to satisfy the accuracy requirements in the double precision arithmetic of the workstation.

## 5. Brief description of Fisher's data used for estimation

In J.R. Fisher's experimental investigation two carbon steels with 0.17 (type $B$) and 0.44 (type $W$) weight percent carbon, respectively, were used for the quantitative studies of microvoid nucleation and growth. The samples were subjected to the following sequence of heat treating operations. Rod sections of approximately 0.0826 m in length were austenitized at 50°C above the $A_3$ temperature for 1.5 hours. The austenitized specimens were then rapidly quenched in ice water in order to obtain fine bainitic or martensitic structures. The quenched rods were then tempered at 700°C for a) 1 hour b) 24 hours and c) 120 hours in order to obtain different particle size distributions in specimens of the same type. The heat treated rods were machined into standard tensile specimens of 0.0254m gage length and 0.0064m diameter. All testing was done at room temperature. Metallographic observations were made on both undeformed and deformed specimens using both optical and electron microscopy. For each specimen, a series of transverse sections was prepared corresponding to successively smaller axial distances from the minimum cross section. Each new section was obtained by grinding to the next premarked position and thus the previous sections were destroyed. Therefore, all data required from a given section had to be obtained before preparation of the succeeding one. Each section was carefully polished and etched after preliminary use of various grades of abrasive papers. The microstructural parameters were determined in both deformed and undeformed specimens. For the deformed specimens the areal density of voids $\eta_A$ and the volume fraction of voids $\xi$ were obtained from transverse sections by standard metallographic techniques performed on scanning electron micrographs taken at a magnification of 2000 times. It is observed in Fisher's experiment that the voids tended to have elliptical cross sections similar to those of the particles, as might be expected since the particles were nucleation sites for these voids. In Fisher's experimental work in the summary it was observed that:

(i) Voids are generally associated with particles of greater than average size. They rarely form at very small, isolated particles, even for the severe state of deformation which exists in the neck of a tensile specimen.

(ii) Particles situated on ferrite grain boundaries are favoured sites for the nucleation of voids.

(iii) Voids often form by decohesion of the interfaces of particles which are closely spaced along the tensile axis.

(iv) The maximum gradient in the void nucleation profile occurs at strains of $\bar{\epsilon}_p = 1.15$ and $\bar{\epsilon}_p = 0.80$ for $B$ and $W$ type specimens respectively.

(v) Voids elongate in the tensile direction but maintain elliptical cross-sections, indicating that plastic hole growth, and not ferrite grain boundary separation, dictates the final void geometry.

(vi) Non-equiaxed or irregularly shaped cementite particles are often subject to internal fracture. The resulting cracks tend to be oriented normally to the tensile direction and may sometimes be associated with boundaries between contiguous particles.

The total volume fraction of voids $\xi$ and the nucleation part of volume fraction of voids $\xi^n$ obtained by Fisher [8] are plotted as the function of equivalent plastic strain $\bar{\epsilon}_p$ in Fig. 1. Since this measure of voids is to be used in our forthcoming analysis, it is worth separating the nucleation part from the full measure of $\xi$. As in Perzyna and Nowak [17] the resulting relationship between the nucleation part of $\xi^n$ and $\bar{\epsilon}_p$ is shown also in Fig. 1.

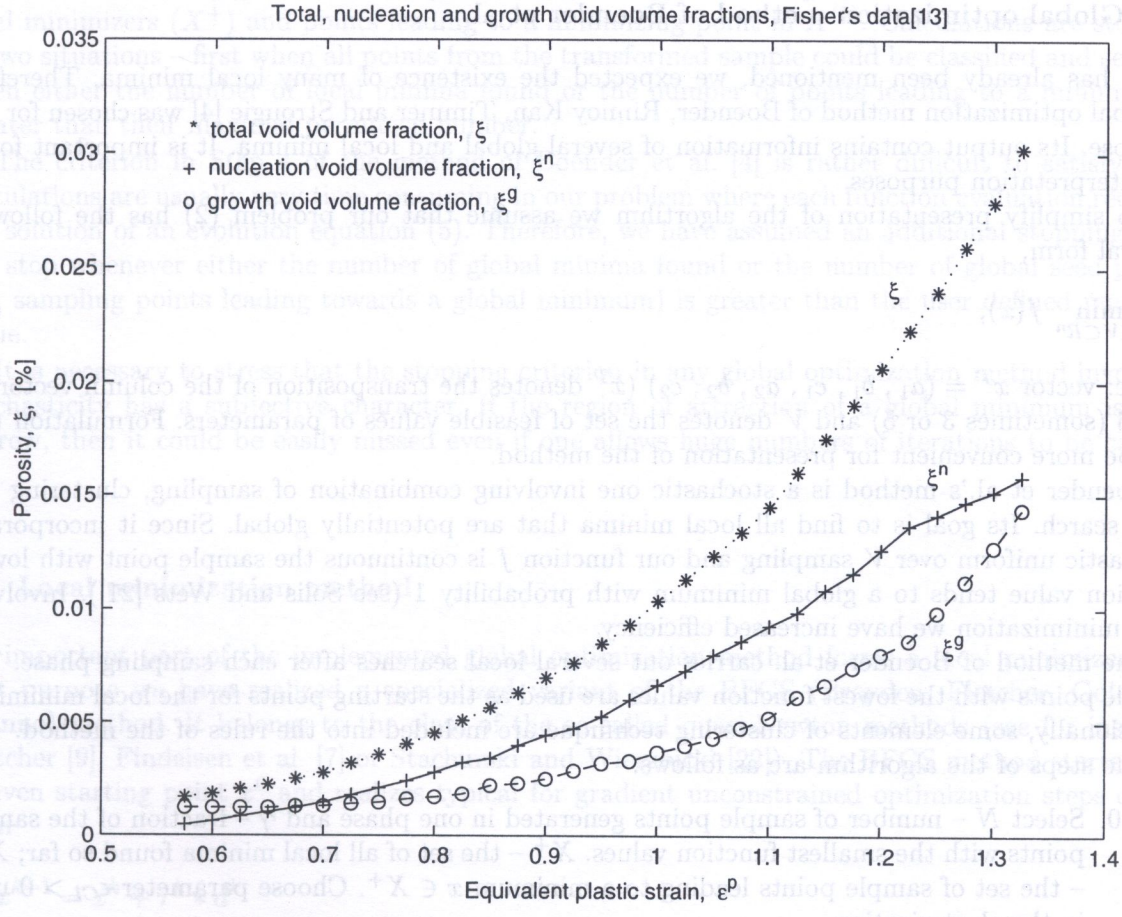


**Fig. 1.** Volume void fraction, $\xi$ (data from Fisher [8] for the B1 type steel) and the calculated nucleation volume void fraction, $\xi^n$, as a function of equivalent plastic strain, $\bar{\epsilon}_p$

In this work, the thorough analysis of the data set was omitted since we decided to concentrate on the computational aspects of the problem of parameter estimation. We were interested in the question of whether it is in fact the global optimization problem. Furthermore, we wanted to obtain the decisive answer to the question of whether the assumed model does fit at all to the given data set.

## 6. Numerical methods

We have decided to use the traditional least squares formulation of the identification problem where the sum of the second power of deviations of the calculated and measured values is minimized (see Section 2). We have expected the existence of many local minima in our problem. Therefore, we have prepared in standard ANSI C language an implementation of the global minimization method of Boender at al. in the form presented in Törn and Žilinskas [23]. It combines the clusterization approach with the local minimization. Locally we have used the BFGS quasi-Newton method with the numerical gradient estimation. The BFGS method is an unconstrained optimization method; however, in our implementation we have introduced box constraints on the parameters.

The example voided media plastic flow model itself is a set of differential coupled equations. Assuming Bridgman solution, we could simplify our set of differential equations.Therefore, to obtain the calculated porosity parameter we had to solve only one poorly conditioned differential evolution equation. We have decided to solve it by means of the Rosenbrock method for stiff differential equations.

### 6.1. Global optimization method of Boender et al.

As it has already been mentioned, we expected the existence of many local minima. Therefore, a global optimization method of Boender, Rinnoy Kan, Timmer and Strougie [4] was chosen for this purpose. Its output contains information of several global and local minima. It is important for us for interpretation purposes.

To simplify presentation of the algortihm we assume that our problem (2) has the following general form,

$$\min_{x \in V \subset R^n} f(x), \tag{18}$$

where: vector $x^T = (a_1, b_1, c_1, a_2, b_2, c_2)$ ($x^T$ denotes the transposition of the column vector $x$), $n = 6$ (sometimes 3 or 5) and $V$ denotes the set of feasible values of parameters. Formulation (18) will be more convenient for presentation of the method.

Boender et al.'s method is a stochastic one involving combination of sampling, clustering and local search. Its goal is to find all local minima that are potentially global. Since it incorporates stochastic uniform over $V$ sampling and our function $f$ is continuous the sample point with lowest function value tends to a global minimum with probability 1 (see Solis and Wets [21]). Involving local minimization we have increased efficiency.

The method of Boender et al. carries out several local searches after each sampling phase. The sample points with the lowest function values are used as the starting points for the local minimizer. Additionally, some elements of clustering technique are included into the rules of the method.

The steps of the algorithm are as follows:

Step 0. Select $N$ – number of sample points generated in one phase and $\gamma$ – fraction of the sample points with the smallest function values. $X^+$ – the set of all local minima found so far; $X^{(1)}$ – the set of sample points leading to a minimum $x \in X^+$. Choose parameter $\epsilon_{Cl} > 0$ used in the clusterization.

Step 1. Select $N$ randomly generated points $x^1, x^2, \ldots, x^N \in V$. Let $f^i = f(x^i)$ for $i = 1, \ldots, N$.

Step 2. Construct the transformed sample by taking the fraction $\gamma$ lowest points of the current sample ($N^+$ denotes their number), performing one step of the steepest descent method and replacing those points by the resulting points. Drop the rest of the points.

Step 3. Apply the clustering procedure to the transformed sample. The elements of $X^+$ (set of global points – local minima found up till now) are first chosen as seed points followed by the elements of $X^{(1)}$ (set of sample points leading to a minimum $x \in X^+$).

If all points $x^1, x^2, \ldots, x^{N^+}$ are classified then STOP, otherwise go to the next step.

Step 4. For $i = 1, \ldots, N^+$ do

if $x^i$ is classified neither to $X^+$ nor to $X^{(1)}$ then

a) apply the local search procedure starting from $x^i$ to obtain $x^{i+}$.

b) if $x^{i+} \in X^+$ then add $x^i$ to $X^{(1)}$ (new seed point leading to an existing minimum),

c) if $x^{i+} \notin X^+$ ($x^{i+}$ is a new local minimum) then add $x^{i+}$ to $X^+$ and $x^i$ to $X^{(1)}$.

Step 5. Return to Step 1.

For clustering, a kind of a nearest neighbour method was used (see Törn and Žilinskas [23]). The unclustered points are added to a cluster, initiated by a seed point either in $X^+$ or in $X^{(1)}$, if the distance to some point in the cluster is less than an a priori given distance $\epsilon_{Cl}$. Hence, accordingly statements $x \in X^+$ and $x \in X^{(1)}$ should be understood in this way. As the result we are storing local minimizers ($X^+$) and points leading to a minimizing point in $X^{(1)}$. Calculations are stopped in two situations – first when all points from the transformed sample could be classified and second, when either the number of local minima found or the number of points leading to a minimum is greater than their maximal permitted number.

The criterion in Step 4 of the method of Boender et al. [4] is rather difficult to satisfy. The calculations are usually very time consuming in our problem where each function evaluation requires the solution of an evolution equation (5). Therefore, we have assumed an additional stopping rule. We stop whenever either the number of global minima found or the number of global seed points (i.e. sampling points leading towards a global minimum) is greater than the user defined maximal value.

It is necessary to stress that the stopping criterion in any global optimization method involving stochasticity has a subjective character. If the region of attraction of a global minimum is very narrow, then it could be easily missed even if one allows huge numbers of iterations to be carried out.

### 6.2. Local minimization method

An important part of the implemented global optimization method forms a local minimizer. For that purpose we have realized a specialized variant of the BFGS (Broyden, Fletcher, Goldfarb, Shanno) method. It belongs to the class of the so-called quasi-Newton methods (see for instance Fletcher [9], Findeisen et al. [7] or Stachurski and Wierzbicki [22]). The BFGS method starts from a given starting point $x^0$ and realizes typical for gradient unconstrained optimization steps of the form

$$x^{k+1} = x^k + \tau^k * d^k \tag{19}$$

where $d^k = -H^k \nabla f(x^k)$ is the search direction and $\tau^k$ is the stepsize coefficient selected in the directional minimization function. It utilizes the gradient and independent variables differences to update the approximation $H^k$ of the inverse of the second order derivative $(\nabla^2 f(x^k))^{-1}$ of the minimized function according to the following formula,

$$H^{k+1} = H^k + \left(1 + \frac{(r^k)^T H^k r^k}{(r^k)^T s^k}\right) \frac{s^k (s^k)^T}{(r^k)^T s^k} - \frac{s^k (r^k)^T H^k + H^k r^k (s^k)^T}{(r^k)^T s^k}, \tag{20}$$

where $r^k = p^{k+1} - p^k$, $s^k = x^{k+1} - x^k$ and $p^k = \nabla f(x^k)$.

Iterations of the local minimizer are stopped when the norm of the gradient (derivative) of function $f$ is smaller than a given accuracy $\epsilon_{\mathrm{BFGS}} > 0$. In the directional minimization we have used successive quadratic approximations of function $\bar{f}(\tau) = f(x^k + \tau * d^k)$. Search along the direction is stopped when the so-called Armijo step-size rule is satisfied, i.e.

$$\frac{|\mathrm{d}\bar{f}(\tau^k)|}{-\mathrm{d}\bar{f}(0)} = \frac{|(\nabla f(x^k + \tau^k d^k))^T d^k|}{-(\nabla f(x^k))^T d^k} \leq \omega, \qquad \text{for some} \quad \omega \in (0,1) \tag{21}$$

Parameters $\epsilon_{\mathrm{BFGS}}$ and $\omega$ are specified by the user.

We have modified this general scheme of the minimizer to take into account box constraints on variables. This is in accordance with the modern optimization routines which are usually implemented so that they minimize a function subject to box constraints, i.e. solve the problem

$$\begin{aligned} &\min_{x \in R^n} \ f(x) \\ &\text{s.t.} \quad x_i^L \leq x \leq x_i^U, \qquad \text{for } i = 1, \ldots, n. \end{aligned} \tag{22}$$

It was also necessary to modify the stopping criterion. The Kuhn–Tucker necessary optimality conditions in the case of box constraints take the form:

(i) the following inequalities should be satisfied on the boundaries

$$\begin{aligned} &\text{if} \quad x_i^{k+1} = x_i^L \quad \text{then} \quad p_i^{k+1} \geq 0, \\ &\text{if} \quad x_i^{k+1} = x_i^U \quad \text{then} \quad p_i^{k+1} \leq 0, \\ &\text{for} \quad i = 1, \ldots, n, \end{aligned}$$

(ii) the norm of the gradient in the subspace of variables that are not on their bounds in the new point $x^{k+1}$ should be equal to 0. Of course, in practice we verify whether it is sufficiently small.

The resulting algorithm is as follows

Step 0. Specify bounds $x^L$ and $x^U$ on variables. Select a feasible starting point $x^0$ satisfying the box constraints. Choose accuracy parameters – $\epsilon_{\mathrm{BFGS}} > 0$, $\omega \in (0,1)$. Calculate values of gradient $p^0$ and function $f^0$ at the starting point $x^0$. Take $H^0 = I$ where $I$ is the identity matrix, $k := 0$.

Step 1. Calculate the current search direction according to the following formula

$$d^k = -H^k p^k.$$

Step 2. Find $\tau \leq 0$ such that the Armijo step-size rule is satisfied, i.e.

$$\frac{|(\nabla f(x^k + \tau^k d^k))^T d^k|}{-(\nabla f(x^k))^T d^k} \leq \omega.$$

Step 3. Calculate the next point

$$x^{k+1} = x^k + \tau^k d^k.$$

and the gradient at the new point $p^{k+1}$.

Step 4. Check the stopping criterion (the Kuhn–Tucker conditions). If the stopping criteria are satisfied then STOP.

Step 5. Compute the gradient $r^k = p^{k+1} - p^k$ and independent variables $s^k = x^{k+1} - x^k$ differences. Update the approximation of the inverse Hessian using formula (20).

Step 6. Set $x^{k+1} = x^k$, $p^{k+1} = p^k$. Increase the iteration index $k$ by one. Calculate $f(x^k)$. Return to Step 1.

Directional minimization implemented in Step 2 is not typical. In fact, we minimize the function $\bar{f}(P(x^k + \tau d^k))$ instead of $\bar{f}(x^k + \tau d^k)$ where $P$ represents the projection operator on the set of feasible points defined by the box constraint. So this means that we maintain the inverse Hessian approximation in the whole space, generate the descent direction in the whole space and carry out the directional minimization in a specific way. It differentiates substantially our approach from the typical active set method for problems with linear constraints.

### 6.3. Integration of the ordinary differential equation

The considered model has the form of an ordinary differential equation. The right-hand side of Eq. (4) contains singularity. Presence of term $\frac{1}{1-\xi}$ causes the right-hand side to vary rapidly when $\xi$ approaches 1. Generally, it has appeared that our equation is stiff and standard Runge–Kutta methods with automatic selection of the step-size coefficients failed in our calculations. Obviously, we could apply a Runge–Kutta method with constant step-size, however we have decided to postpone that possibility due to the difficulties with the accuracy specification.

As a result, we have assumed that our equation is stiff and selected a Rosenbrock method for solving stiff sets of ordinary differential equations (see Numerical Recipes [18]).

## 7. Numerical results

In this section the results of parameter estimation will be presented. It is impossible to present all aspects of the calculations in a short paper. Therefore we restrict the full presentation of all minima found only to some selected sectors and to indicate in this way the characteristic elements in the behavior of the program used for calculations.

The results are collected in Tables 1a, 1b, 2a, 2b, 3a and 3b. Each line of Tables 1a, 2a and 3a contain the following information about a minimum (the functional values and the corresponding values of parameters) and Tables 1b, 2b and 3b contain frequently used statistical information: standard deviation $s_e$,

$$s_e^2 = \frac{\left[\sum_{i=1}^{M}(Y_i - \tilde{Y}_i)^2\right]}{M}, \tag{23}$$

where $M$ is the number of observations, $Y_i$ are the observed values of the output and $\tilde{Y}_i = F(\bar{\epsilon}_{p^i}, x)$ for $i = 1, \ldots, M$ are the calculated values of the output; weighted standard error $s_{ew} = \frac{s_e}{\bar{Y}}$ (where

**Table 1.** a) Results for Case I, b) Statistical results for Case I; $\boldsymbol{h}$ – Gauss function with $a_1$, $b_1$ and $c_1$ ; $\boldsymbol{g}$ – exponent function with $a_2$, $b_2$ and $c_2$

a)

| | $a_1$ | $b_1$ | $c_1$ | $a_2$ | $b_2$ | $c_2$ | $f$ |
|---|---|---|---|---|---|---|---|
| 1 | 1.241248e−2 | 2.678213e−1 | 1.027411 | 1.325793 | 9.582941e−2 | 1.259289e−1 | 1.765069e−7 |
| 2 | 1.618972e−2 | 2.859666e−1 | 1.082775 | 1.112041 | 1.767954e−1 | 9.087024e−2 | 1.822506e−7 |
| 3 | 1.899431e−2 | 3.425415e−1 | 1.142513 | 1.133089 | 1.643974e−1 | 2.994370e−2 | 2.865987e−7 |
| 4 | 2.313844e−2 | 3.740792e−1 | 1.207354 | 1.274346 | 1.000000e−2 | 4.404039e−2 | 3.527062e−7 |
| 5 | 1.059191e−2 | 2.616696e−1 | 0.998871 | 1.208910 | 2.481699e−1 | 1.142236e−1 | 3.907237e−7 |
| 6 | 2.661567e−2 | 3.937362e−1 | 1.247294 | 1.219216 | 1.000000e−2 | 7.691108e−2 | 3.932288e−7 |
| 7 | 2.063523e−2 | 3.204170e−1 | 1.130544 | 1.078865 | 1.056202e−1 | 1.380099e−1 | 7.410887e−7 |
| 8 | 1.866313e−2 | 4.277909e−1 | 1.167299 | 1.314933 | 1.033405e−1 | 1.634633e−1 | 1.113769e−6 |
| 9 | 2.046574e−2 | 4.648678e−1 | 1.210805 | 1.333576 | 9.190177e−2 | 1.798287e−1 | 1.310531e−6 |
| 10 | 2.073439e−2 | 4.322754e−1 | 1.196344 | 1.321222 | 5.280925e−2 | 1.484434e−1 | 1.483868e−6 |

b)

| | $s_e$ | $s_{ew}$ | $r_{Y\tilde{Y}}$ | $t_{\text{Student}}$ |
|---|---|---|---|---|
| 1 | 5.883563e−9 | 6.698777e−3 | 9.999611e−1 | −5.443949e−1 |
| 2 | 6.075018e−9 | 6.811169e−3 | 9.999593e−1 | −4.501236e−2 |
| 3 | 9.553290e−9 | 8.519307e−3 | 9.999484e−1 | −1.720928 |
| 4 | 1.175687e−8 | 9.452369e−3 | 9.999318e−1 | −1.439367 |
| 5 | 1.302412e−8 | 9.968912e−3 | 9.999153e−1 | −2.441371e−1 |
| 6 | 1.310763e−8 | 9.961483e−3 | 9.999451e−1 | −2.599829 |
| 7 | 2.470296e−8 | 1.364173e−2 | 9.999123e−1 | −3.064458 |
| 8 | 3.712562e−8 | 1.674371e−2 | 9.998092e−1 | −1.895669 |
| 9 | 4.368438e−8 | 1.816057e−2 | 9.997675e−1 | −1.768998 |
| 10 | 4.946226e−8 | 1.943638e−2 | 9.998754e−1 | 3.333778e−3 |

$\bar{Y} = \frac{\left[\sum_{i=1}^{M} Y_i\right]}{M}$ is the mean value of the observed output); correlation coefficient $r_{Y\tilde{Y}}$ between the observed and calculated output:

$$r_{Y\tilde{Y}} = \frac{\sum_{i=1}^{M}(Y_i - \bar{Y}_i)(\tilde{Y}_i - \bar{\tilde{Y}})}{\left[\sum_{i=1}^{M}(Y_i - \bar{Y})^2\right]^{\frac{1}{2}}\left[\sum_{i=1}^{M}(\tilde{Y}_i - \bar{\tilde{Y}})^2\right]^{\frac{1}{2}}}, \tag{24}$$

(where $\bar{\tilde{Y}} = \frac{\left[\sum_{i=1}^{M} \tilde{Y}_i\right]}{M}$ is the mean value of the calculated output); values of the t-criterion, i.e.

$$t_s = \frac{\bar{z}}{S_z}\sqrt{M-1}, \tag{25}$$

where

$$z_i = Y_i - \tilde{Y}_i, \qquad \bar{z} = \frac{\left[\sum_{i=1}^{M} z_i\right]}{M}, \qquad S_z^2 = \frac{\left[\sum_{i=1}^{M} z_i^2 - \frac{(\sum_{j=1}^{M} z_i)^2}{M}\right]}{(M-1)}. \tag{26}$$

**Table 2.** a) Results for Case II, b) Statistical results for Case II; $\boldsymbol{h}$ – powered exponent function with $a_1$, $b_1$ and $c_1$; $\boldsymbol{g}$ – square function with $a_2$, $b_2$ and $c_2$

a)

| | $a_1$ | $b_1$ | $c_1$ | $a_2$ | $b_2$ | $c_2$ | $f$ |
|---|---|---|---|---|---|---|---|
| 1 | 9.046740e−3 | 1.293135 | 1.293855 | 4.231977e−1 | 2.668830e−1 | 9.615650e−1 | 1.505891e−6 |
| 2 | 8.308979e−3 | 1.226094 | 1.399982 | 4.168414e−1 | 1.109089e−1 | 9.512816e−1 | 1.513673e−6 |
| 3 | 8.909187e−3 | 1.125933 | 1.182042 | 5.315358e−1 | 3.861025e−1 | 8.901577e−1 | 1.876370e−6 |
| 4 | 8.844457e−3 | 1.264524 | 1.215909 | 5.303751e−1 | 3.683762e−1 | 8.897531e−1 | 2.540529e−6 |
| 5 | 9.041638e−3 | 1.271911 | 1.130437 | 5.976880e−1 | 1.483844e−1 | 1.000000 | 2.640661e−6 |
| 6 | 9.697199e−3 | 1.283282 | 1.295817 | 3.757060e−1 | 2.567556e−1 | 8.894673e−1 | 4.105814e−6 |
| 7 | 1.546990e−2 | 1.153664 | 1.000407 | 1.023656e−1 | 1.895401e−1 | 9.550388e−1 | 2.940338e−5 |
| 8 | 1.472176e−2 | 1.146364 | 1.234183 | 1.108397e−1 | 2.367317e−1 | 9.367317e−1 | 2.186483e−4 |
| 9 | 2.053909e−2 | 1.084802 | 1.000000 | 5.236047e−2 | 1.000000e−1 | 9.046464e−1 | 4.711965e−4 |
| 10 | 1.604174e−2 | 1.159577 | 1.255324 | 1.732044e−1 | 3.212940e−1 | 8.212940e−1 | 7.884759e−4 |

b)

| | $s_e$ | $s_{ew}$ | $r_{Y\tilde{Y}}$ | $t_{\text{Student}}$ |
|---|---|---|---|---|
| 1 | 5.019637e−8 | 1.947700e−2 | 9.997308e−1 | −1.482688 |
| 2 | 5.045577e−8 | 1.950426e−2 | 9.997362e−1 | −1.846877 |
| 3 | 6.254566e−8 | 2.169656e−2 | 9.996820e−1 | −1.890806 |
| 4 | 8.468432e−8 | 2.522520e−2 | 9.995007e−1 | −1.799602 |
| 5 | 8.802202e−8 | 2.585770e−2 | 9.994130e−1 | −5.581049e−1 |
| 6 | 1.368605e−7 | 3.142103e−2 | 9.998197e−1 | −1.063759e+1 |
| 7 | 9.801125e−7 | 8.258295e−2 | 9.975251e−1 | −3.494708 |
| 8 | 7.288275e−6 | 1.945753e−1 | 9.988241e−1 | −1.098827e+1 |
| 9 | 1.570655e−5 | 2.635223e−1 | 9.966151e−1 | −1.143741e+1 |
| 10 | 2.628253e−5 | 3.256617e−1 | 9.993503e−1 | −8.153208 |

This last value allows us to test the hypothesis that the expectation of the error $\mathbf{z} = \mathbf{Y} - \tilde{\mathbf{Y}}$ is equal to zero under the assumption that the error distribution is normal and $\sigma^2$ is unknown (see Afifi and Azen [1]). In such case $t_s$ determined by formula (25) has Student t-distribution with $M-1$ degrees of freedom. Let $\theta = E(z)$ be the expectation of $z$. We test the $H_o$ hypothesis that the expectation $\theta$ is equal to zero, i.e. $H_o : \theta = 0$. As the alternative hypothesis $H_1 : \theta \neq 0$ is used. Then critical probability ($P$–value) is $P = 2Pr(t(\nu) > |t_o|)$.

Hypothesis $H_o$ is rejected if $P < \kappa$, where $\kappa$ denotes the level of significance. Instead of it one can check equivalently whether $t_s$ belongs to the interval $\left(-t_{1-\kappa/2}(M-1)\,,\, t_{\kappa/2}(M-1)\right)$, where $t_{1-x/2}(M-1)$ denotes the critical value with the level of significance equal $\kappa$. For $M = 30$ and the level of significance $\kappa = 0.1$ the critical value is $t_{1-\kappa/2}(29) = 1.697$.

Tables 1a, 2a and 3a contain the global minima for each interval in Cases I, II and III, respectively. They are presented here to show the variety of possible solutions to the minimization of the mean squares function if the parameters appear in the model nonlinearly. It seems that the presented numerical results justify our hypothesis about the possibility of existence of many local minima in the considered problem.

**Table 3.** a) Results for Case III, b) Statistical results for Case III; $\boldsymbol{h}$ – shifted hyperbolic tangent function with $a_1$, $b_1$ and $c_1$; $\boldsymbol{g}$ – hyperbolic function with $a_2$, $b_2$ and $c_2$

a)

| | $a_1$ | $b_1$ | $c_1$ | $a_2$ | $b_2$ | $c_2$ | $f$ |
|---|---|---|---|---|---|---|---|
| 1 | 2.613975e−2 | 2.832813 | −2.590365 | 2.427288 | 4.011257 | 0.0 | 1.815666e−7 |
| 2 | 2.576480e−2 | 2.921375 | −2.645284 | 2.012904 | 3.525663 | 0.0 | 1.892425e−7 |
| 3 | 2.563549e−2 | 2.868868 | −2.592992 | 2.288288 | 3.864572 | 0.0 | 2.319430e−7 |
| 4 | 2.529889e−2 | 2.500000 | −2.324462 | 2.404474 | 3.718682 | 0.0 | 3.750747e−7 |
| 5 | 1.573926e−2 | 2.746651 | −2.271808 | 2.500000 | 3.138761 | 0.0 | 3.625997e−6 |
| 6 | 2.937236e−2 | 3.932955 | −3.413079 | 1.439093 | 3.878186 | 0.0 | 6.229797e−6 |
| 7 | 7.227557e−2 | 2.500000 | −2.927299 | 1.000000 | 4.053395 | 0.0 | 7.238592e−6 |
| 8 | 3.851723e−2 | 2.805516 | −2.971102 | 1.748733 | 3.018904 | 0.0 | 1.846002e−5 |
| 9 | 1.000000e−1 | 2.504127 | −3.246445 | 1.937504 | 4.499889 | 0.0 | 3.302284e−5 |
| 10 | 5.943800e−2 | 2.500000 | −2.959125 | 1.679795 | 3.071635 | 0.0 | 3.587069e−5 |

b)

| | $s_e$ | $s_{ew}$ | $r_{Y\tilde{Y}}$ | $t_{\text{Student}}$ |
|---|---|---|---|---|
| 1 | 6.052220e−9 | 6.792539e−3 | 9.999608e−1 | −7.209498e−1 |
| 2 | 6.308083e−9 | 6.942618e−3 | 9.999573e−1 | 1.785760e−1 |
| 3 | 7.731434e−9 | 7.654595e−3 | 9.999612e−1 | −3.094756 |
| 4 | 1.250249e−8 | 9.722458e−3 | 9.999404e−1 | −3.211188 |
| 5 | 1.208666e−7 | 3.096390e−2 | 9.995494e−1 | 4.160066 |
| 6 | 2.076599e−7 | 3.896229e−2 | 9.993616e−1 | −3.538134 |
| 7 | 2.412864e−7 | 4.307644e−2 | 9.992222e−1 | 4.267485e−1 |
| 8 | 6.153340e−7 | 7.086173e−2 | 9.977709e−1 | 2.859486 |
| 9 | 1.100761e−6 | 9.580245e−2 | 9.958560e−1 | 2.805669 |
| 10 | 1.195690e−6 | 9.552565e−2 | 9.967818e−1 | −2.069778e−2 |

## 8. Conclusions and comments

We expected that the problem of estimation of parameters appearing nonlinearly in a model is in fact a global optimization problem. The results presented in our paper fully justify the hypothesis that parameter estimation is a global optimization problem in this case. Our calculations have led to finding several local minima in all cases. The best fitting error is of order $10^{-7}$ (see Fig. 2). However, we have found several other local minima of the least squares function which are slightly worse with respect to the fitting error. This fitting error is also relatively good (from $10^{-6}$ till $10^{-5}$) and the parameters are reasonable from the mechanical point of view.

Therefore, we may claim that our approach is successful and we have proved experimentally the existence of many local solutions of the identification problem. An open question is which of them should be chosen.

In the paper only some selected estimation results are presented. Broader presentation covering more examples of material functions and deeper analysis of the identification results shall be pursued in another forthcoming paper.

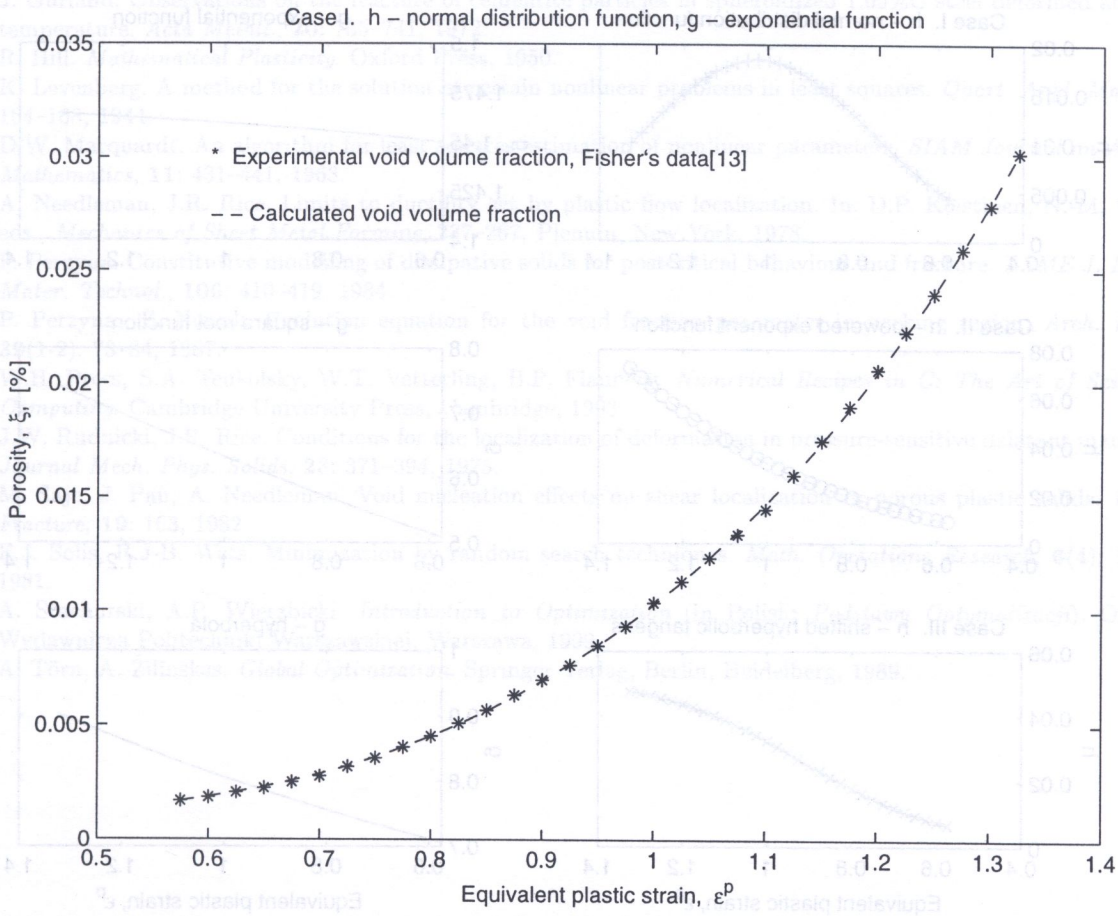


**Fig. 2.** Comparison of computed and experimental values of total porosity versus equivalent plastic strain

The estimated material functions $\boldsymbol{h}$ and $\boldsymbol{g}$ are plotted in Fig. 3 for our optimization approach. We would like to stress our material function was determined with following important assumptions. The matrix material is plastically incompressible, $\dot{\rho}_m = 0$ and the elastic part of a strain rate tensor is neglected, $D_{ij} = D^p_{ij}$. The shape of the material function $\boldsymbol{h}$ in these figures is in agreement with the material function proposed by Chu and Needleman [6]. However, the growth material function $\boldsymbol{g}$ as in Perzyna and Nowak [17] can be not constant and has the shape of an exponential function. Another open question is the formulation of the minimized function. It is not clear whether the euclidean distance in the space of observations is the best measure. One can use in Eq. (2) the $l_1$-norm or $l_\infty$-norm or any other suitable norm. The problem will then be nondifferentiable and will have completely different features but it can also be handled by our computational program. It is the next possibility we intend to study — the use of other measures of deviations of the calculated output from the measured one. The existence of many local minima is also expected in this case.

The results prove also something more. It is doubtful whether the global optimum should be chosen in all cases since there frequently exist other completely different local minima with similar standard error values, each of them acceptable from the statistical point of view. The problem of selecting the "best" solution requires further investigation. To determine uniquely the material functions $\boldsymbol{h}$ and $\boldsymbol{g}$ it is most probably necessary to include an additional formula mutually connecting those functions. At the present stage of research only mechanical interpretations and conditions may suggest the best choice.

We have got exclusively porosity data for carbon steel metal specimen. Unfortunately any data base containing laboratory experiment results for other materials is not available for us and we are not able to carry out laboratory experiments ourselves. We have to rely on data published in

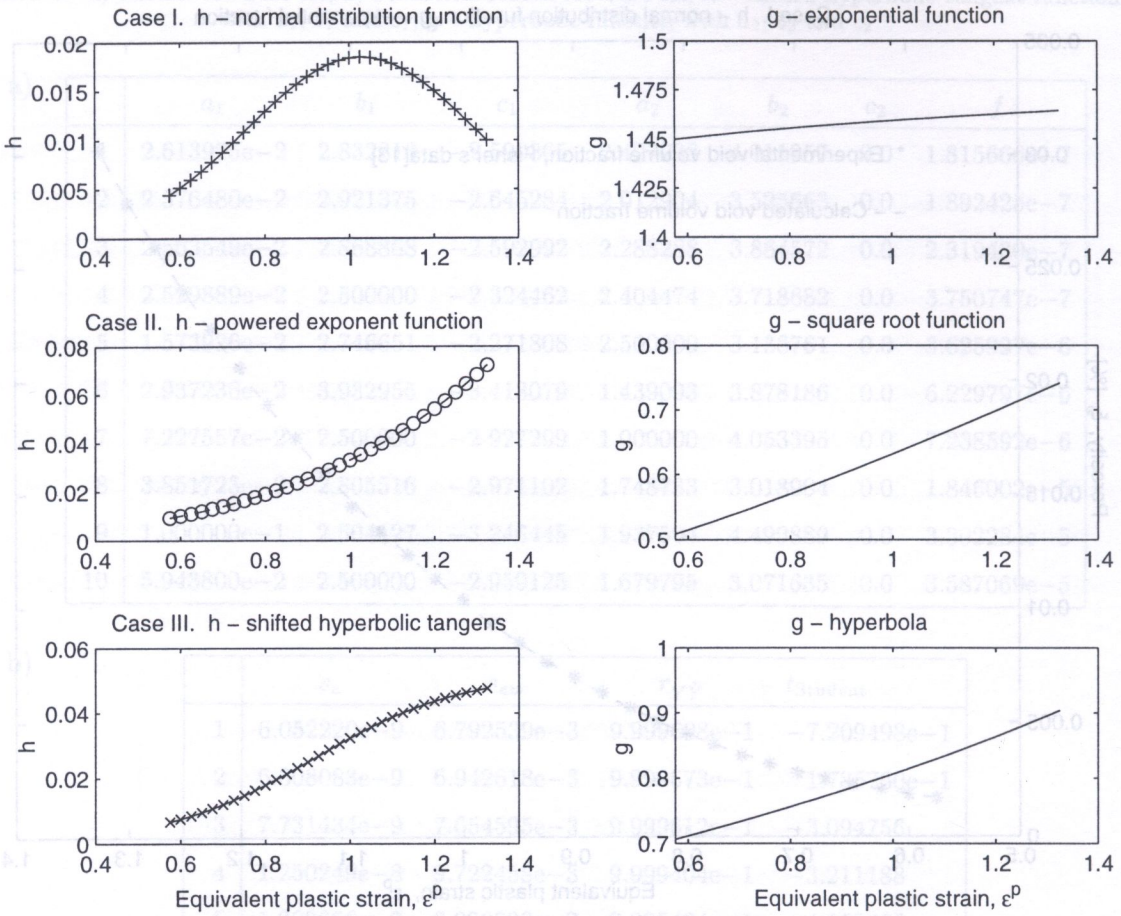


**Fig. 3.** Computed nucleation material function $h$ and computed growth material function $g$ as functions of equivalent plastic strain $\bar{\epsilon}_p$ in Cases I, II and III

the literature, which are very limited. Currently we continue our work assuming other forms of the porosity evolution equation. The results shall be presented in a forthcoming paper. We shall apply our identification code to parameter identification for other elastoplastic materials if we find appropriate porosity experimental data.

## References

[1] A.A. Afifi, S.P. Azen. *Statistical Analysis. A Computer Oriented Approach.* Academic Press, New York, 1979.

[2] A.S. Argon, J. Im. Separation of second-phase particles in spheroidized 1045 steel, Cu-0.6 pct Cr alloy and maraging steel in plastic straining. *Metall. Trans.*, **6A**: 839–851, 1975.

[3] A.S. Argon, J. Im, R. Safoglu. Cavity formation from inclusions in ductile fracture. *Metall. Trans.*, **6A**: 825–838, 1975.

[4] C.G. Boender, A.H.G. Rinnooy Kan, L. Strougie, G.T. Timmer. A stochastic method for global optimization. *Mathematical Programming*, **22**: 125–140, 1982.

[5] P.W. Bridgman. *Studies in Large Plastic Flow and Fracture.* McGraw-Hill, 1952.

[6] C.C. Chu, A. Needleman. Void nucleation effects in biaxially stretched sheets. *Trans. ASME, J. Engng. Materials and Technology*, **102**: 249–256, July 1980.

[7] W. Findeisen, J. Szymanowski, A. Wierzbicki. *Theory and Computational Methods of Optimization* (in Polish: *Teoria i Metody Obliczeniowe Optymalizacji*). PWN, Warszawa, 1977.

[8] J.R. Fisher. Void nucleation in spheroidized steels during tensile deformation. Ph.D. Thesis, Brown University, June 1980.

[9] R. Fletcher. *Practical Methods of Optimization*, Second edition. John Wiley & Sons, Chichester, 1987.

[10] A.L. Gurson. Continuum theory of ductile rupture by void nucleation and growth. Part 1. Yield criteria and flow rules for porous ductile media. *Trans. ASME, J. Engng. Materials and Technology*, **99**: 2–15, 1977.

[11] J. Gurland. Observations on the fracture of cementite particles in spheroidized 1.05%C steel deformed at room temperature. *Acta Metall.*, **20**: 735–741, 1972.
[12] R. Hill. *Mathematical Plasticity.* Oxford Press, 1950.
[13] K. Levenberg. A method for the solution of certain nonlinear problems in least squares. *Quart. Appl. Math.*, **2**: 164–168, 1944.
[14] D.W. Marquardt. An algorithm for least squares estimation of nonlinear parameters. *SIAM Journal on Applied Mathematics*, **11**: 431–441, 1963.
[15] A. Needleman, J.R. Rice. Limits to ductility set by plastic flow localization. In: D.P. Koistinen, N.-M. Wang, eds., *Mechanics of Sheet Metal Forming*, 237–267. Plenum, New York, 1978.
[16] P. Perzyna. Constitutive modelling of dissipative solids for postcritical behaviour and fracture. *ASME J. Engng. Mater. Technol.*, **106**: 410–419, 1984.
[17] P. Perzyna., Z. Nowak. Evolution equation for the void fraction parameter in necking region. *Arch. Mech.*, **39**(1-2): 73–84, 1987.
[18] W.H. Press, S.A. Teukolsky, W.T. Vetterling, B.P. Flannery. *Numerical Recipes in C: The Art of Scientific Computing.* Cambridge University Press, Cambridge, 1993.
[19] J.W. Rudnicki, J.R. Rice. Conditions for the localization of deformation in pressure-sensitive delatant materials. *Journal Mech. Phys. Solids*, **23**: 371–394, 1975.
[20] M. Saje, J. Pan, A. Needleman. Void nucleation effects on shear localization in porous plastic solids. *Int. J. Fracture*, **19**: 163, 1982.
[21] F.J. Solis, R.J-B. Wets. Minimization by random search techniques. *Math. Operations Research*, **6**(4): 19–30, 1981.
[22] A. Stachurski, A.P. Wierzbicki. *Introduction to Optimization* (in Polish: *Podstawy Optymalizacji*). Oficyna Wydawnicza Politechniki Warszawskiej, Warszawa, 1999.
[23] A. Törn, A. Žilinskas. *Global Optimization.* Springer Verlag, Berlin, Heidelberg, 1989.